EPiC Series in Engineering

Volume 5, 2023, Pages 23–35

Proceedings of International Symposium on Applied Science 2022


# Dynamic Analysis In Functionally Graded Material Plate Using A Meshless Method

Manh Dung Dinh[1,2], My Hien Nguyen Thi[3] and Thanh Nha Nguyen[1,2*]

[1] Department of Engineering Mechanics, Faculty of Applied Sciences, Ho Chi Minh City University of Technology (HCMUT), 268 Ly Thuong Kiet Street, District 10, Ho Chi Minh City, Viet Nam

[2] Vietnam National University Ho Chi Minh City, Linh Trung Ward, Thu Duc City, Ho Chi Minh City, Viet Nam

[3]Institute of Transport and Environment Research, Ho Chi Minh City University of Transport, 2 Vo Oanh Street, Ward 25, Binh Thanh District, Ho Chi Minh City, Vietnam.

nhanguyen@hcmut.edu.vn

**Abstract**

Functionally graded materials (FGMs) are complicated composites created using the concept of continuous variation of material property in one or more predetermined directions. FGMs have been used in the manufacturing of structural parts that are subjected to non-uniform functioning requirements in recent years. In a thermal protection system, for example, FGMs combine the benefits of traditional ceramics, such as corrosion and heat resistance, with those of metal, such as mechanical strength and rigidity. They are common in engineering practice, so static analysis and dynamic analysis for FGM plate structures are necessary. The radial point interpolation method (RPIM) meshless method has been used based on the point interpolation method (PIM) by including the radial basis function (RPF) in the interpolation formulation and has shown good performance in computational engineering. One of the advantages of this method is that it satisfies the Kronecker's delta function, which overcomes the limitations of critical boundary conditions for the traditional meshless method. Furthermore, RPIM shape function satisfies the high-order continuity constraint, which the low-order finite element methods (FEM) method does not. This paper presents a meshless approach for the static and dynamic analysis of FGM plates whose material properties vary through the thickness. Numerical examples are solved and the results are compared with reference solutions or the results of FEM given by SOMSOL program to confirm the accuracy of the proposed method.

* Corresponding author

T.N. Tran, Q.K. Le, T.T. Truong, T.N. Nguyen and H.N. Huynh (eds.), ISAS 2022 (EPiC Series in Engineering, vol. 5), pp. 23–35

# 1 Introduction

In computational mechanics, the study of structural statics and dynamics issues is extremely important and its analysis necessitates greater modeling work due to the interaction of many various variables under sophisticated external loadings. Due to the numerous requirements of engineering applications in reality, finding an analytical solution is typically challenging and impossible in most of cases. As a result, numerical computational methods emerge as a viable option for estimating a solution. The finite element method (FEM), for example [1,2], emerged as a solution to this problem and has since become the most widely used numerical tool for solving it. Such numerical computing approaches are now inescapable in today's world. Meshfree or meshless approaches, such as [3–5], have evolved as an alternative in the last two decades, where a collection of distributed "nodes" in the domain is employed instead of a set of elements "or mesh" as in the FEM. Meshfree approaches don't usually require meshing. It's worth noting that the idea of meshing here differs from the concept of background cells, which are often required for doing domain integrations. Another notion is "really" meshfree or meshless approaches, in which no meshing is required at all, including the background cells for domain integrations, as shown in [5–7]. The meshless local Petrov-Galekin (MLPG) approach, created by the previous author, is used to analyze static, dynamic, and fracture issues in nonhomogeneous, orthotropic, functionally graded materials, Reissner–Mindlin and laminated plates [8–12], as well as Radial basis functions (RBF) (Wang and GR Liu, 2000; GR Liu, 2002) have often been used in MFree methods [13]. The Uflyand-Mindlin theory of vibrating plates is an extension of the Kirchhoff–Love plates theory that considers shear deformations over a plate's thickness. Yakov Solomonovich Uflyand [14] (1916-1991) proposed the hypothesis in 1948, and Raymond Mindlin [15] proposed it in 1951, with Mindlin citing Uflyand's work. As a result, we must refer to this theory as the Uflyand-Mindlin plate theory, as done in Elishakoff's handbook [16] and publications by Andronov [17], Elishakoff, Hache, and Challamel [18], Loktev [19], Rossikhin and Shitikova [20], and Wojnar [21]. Elishakoff [22] proposed in 1994 that the fourth-order time derivative in Uflyand-Mindlin equations be ignored. Eric Reissner offered a similar, but not identical, idea in a static context in 1945 [23]. The Uflyand-Mindlin plate theory is applied to thick plates, as the shear deformation and rotary inertia effects can be included. The first-order shear deformation theory of plates is known as the Uflyand-Mindlin theory because a first-order shear deformation theory calls for a linear displacement variation throughout the thickness.

# 2 FGM plates

FGMs are mathematically represented as a continuous variation of mechanical characteristics along the thickness direction. There are several types of FGMs, but the power-law distribution, which is valid for the elastic modulus E and material density ρ[1, 2], is the most widely used formula. The power-law distribution is given by for two material characteristics P1 and P2 as the material at the top (material 1) and bottom (material 2) of the two faces of the beam or plate.

$$\begin{aligned} P(z) &= (P_1 - P_2) f(z) + P_2 \\ \rho(z) &= (\rho_1 - \rho_2) f(z) + \rho_2 \end{aligned} \tag{1}$$

where

$$f(z) = \left(1/2 + z/h\right)^n \tag{2}$$

and n is the power-law index, represents an increase in the proportion of the volume fraction; z is the coordinate variable in thickness. $-0.5h < z < 0.5h$ .

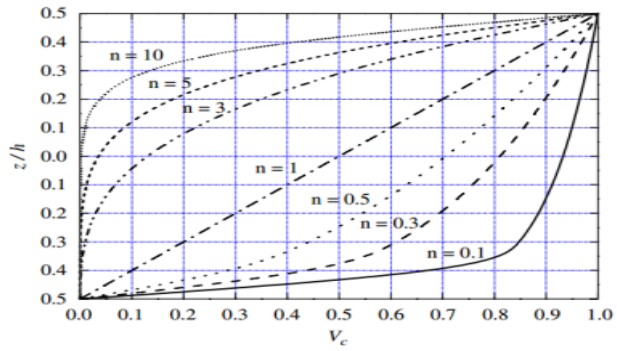


**Figure 1:** Relationship between f(z) and thickness ratio z/h by index n

Figure 1 shows the change of the component volume, including *f (z)* with respect to the FGM plate thickness ratio when the *n*-value changes. For very large values n > 100, *f (z)* is very small - it can be considered that the material of the plate consists only of metal. For very small n values, n < 0.01- can be considered as the material of the plate consisting only of ceramic. The combination of metal and ceramic materials is linear when n = 1.

The deflection of the plate **FGM** is still represented by the deflection at the neutral plane of the plate, and is denoted by *W*. the vecter displacements can the expressed as

$$\begin{Bmatrix} u \\ v \\ w \end{Bmatrix} = \begin{bmatrix} 0 & z & 0 \\ 0 & 0 & z \\ 1 & 0 & 0 \end{bmatrix} \begin{Bmatrix} w \\ \varphi_x \\ \varphi_y \end{Bmatrix} = \mathbf{L}_u \mathbf{d} \tag{3}$$

Where $\varphi_x, \varphi_y$ denote rotations of the cross section of plate about the $Y$ and $X$ axes, recpectively.

The linear strains in plate **FGM** are as follows

$$\begin{Bmatrix} \varepsilon_x \\ \varepsilon_y \\ \gamma_{xy} \\ \gamma_{xx} \\ \gamma_{yz} \end{Bmatrix} = \begin{bmatrix} 0 & z\partial/\partial x & 0 \\ 0 & 0 & z\partial/\partial y \\ 0 & z\partial/\partial y & z\partial/\partial x \\ \partial/\partial x & 1 & 0 \\ \partial/\partial y & 0 & 1 \end{bmatrix} \begin{Bmatrix} w \\ \varphi_x \\ \varphi_y \end{Bmatrix} = \mathbf{L}\mathbf{d} \tag{4}$$

By simply removing the components $\sigma_{zz}$ for the isotropic materials, the stresses can be expressed as

$$\begin{Bmatrix} \sigma_x \\ \sigma_y \\ \tau_{xy} \\ \tau_{xz} \\ \tau_{yz} \end{Bmatrix} = \begin{bmatrix} Q_{11} & Q_{12} & 0 & 0 & 0 \\ Q_{12} & Q_{11} & 0 & 0 & 0 \\ 0 & 0 & Q_{66} & 0 & 0 \\ 0 & 0 & 0 & KQ_{66} & 0 \\ 0 & 0 & 0 & 0 & KQ_{66} \end{bmatrix} \begin{Bmatrix} \varepsilon_x \\ \varepsilon_y \\ \gamma_{xz} \\ \gamma_{yz} \\ \gamma_{yz} \end{Bmatrix} \tag{5}$$

where $K$ is the shear effectiveness factor, $K = 5/6$ for Uflyand-Mindlin plate, $v$ is Poisson's ratio, and $E$ is Young's modulus, and

$$Q_{11} = \frac{E(z)}{1-v^2}; \quad Q_{12} = v\frac{E(z)}{1-v^2} = vQ_{11}; \quad Q_{66} = \frac{E(z)}{2(1-v)} = \frac{1-v}{2}Q_{11} \tag{6}$$

The stiffness coefficients for the Mindlin plate can be calculated as

$$A_{11} = \int_{-h/2}^{h/2} Q_{11}dz = \frac{E_2}{1-v^2}\left(\frac{M+n}{n+1}\right) \tag{7}$$

$$A_{12} = \int_{-h/2}^{h/2} Q_{12}dz = \int_{-h/2}^{h/2} \frac{vE(z)}{1-v^2}dz = vA_{11} \tag{8}$$

$$A_{66} = \int_{-h/2}^{h/2} Q_{66}dz = \int_{-h/2}^{h/2} \frac{E(z)}{2(1+v)}dz = \frac{1-v}{2}A_{11} \tag{9}$$

where M = $E_1/E_2$. The other coefficients are given by

$$D_{11} = \int_{-h/2}^{h/2} z^2 Q_{11}dz = \frac{E_2 h^3}{1-v^2}\left(\frac{(M-1)\left(2+n+n^2\right)}{4(n+1)(n+2)(n+3)} + \frac{1}{12}\right) \tag{10}$$

$$D_{12} = vD_{11}; \quad D_{66} = \frac{1-v}{2}D_{11} \tag{11}$$

$$I_i = \int_{-h/2}^{h/2} \rho(z)z^i dz = \int_{-h/2}^{h/2} \left(\left(\rho_1 - \rho_2\right)f(z) + \rho_2\right)z^i dz \tag{12}$$

$$I_0 = \frac{(\rho_1 - \rho_2)h}{n+1} + \rho_2 h; \quad I_2 = \frac{(\rho_1 - \rho_2)h^3(2+n+n^2)}{4(n+1)(n+2)(n+2)} + \rho_2\frac{h^3}{12} \tag{13}$$

In order to facilitate the calculation, presentation of formulas as well as program development, in this paper, the authors have separated into two parts called bending and shear. Strains are defined as

$$\boldsymbol{\varepsilon}_f = z\mathbf{B}_f\mathbf{d}, \quad \boldsymbol{\varepsilon}_c = \mathbf{B}_c\mathbf{d} \tag{14}$$

The strain-displacement matrices for bending and shear contributions are obtained by derivation of the shape functions by

$$\mathbf{B}_f = \begin{bmatrix} 0 & \frac{\delta}{\delta x} & 0 \\ 0 & 0 & \frac{\delta}{\delta y} \\ 0 & \frac{\delta}{\delta y} & \frac{\delta}{\delta x} \end{bmatrix}; \quad \mathbf{B}_c = \begin{bmatrix} \frac{\delta}{\delta x} & 1 & 0 \\ \frac{\delta}{\delta y} & 0 & 1 \end{bmatrix} \tag{15}$$

Where

$$\mathbf{d} = \begin{Bmatrix} w_i & \theta_{xi} & \theta_{yi} \end{Bmatrix} \tag{16}$$

We then obtain the plate strain energy as

$$\mathbf{U}^e = \frac{1}{2}\mathbf{d}^{eT}\int_{\Omega^e}\int_z \mathbf{B}_f^T\mathbf{D}_f\mathbf{B}_f dzd\Omega^e\mathbf{d}^e + \frac{K}{2}\mathbf{d}^{eT}\int_{\Omega^e}\int_z \mathbf{B}_c^T\mathbf{D}_c\mathbf{B}_c dzd\Omega^e\mathbf{d}^e \tag{17}$$

where $\partial\Omega$ represents the boundary of the domain $\boldsymbol{\Omega}$.

$\mathbf{D}_f$ and $\mathbf{D}_c$ are the bending and shear stiffness matrices in the form

$$\mathbf{D}_f = \begin{bmatrix} D_{11} & D_{12} & 0 \\ D_{12} & D_{11} & 0 \\ 0 & 0 & D_{66} \end{bmatrix}; \quad \mathbf{D}_S = kapaA_{66} \begin{bmatrix} 1 & 0 \\ 0 & 1 \end{bmatrix} \tag{18}$$

where *kapa* is

$$kapa = \frac{5(1+nu)}{6+5nu} \tag{19}$$

The stiffness matrix of the Mindlin plate is then obtained as

$$\mathbf{K}^e = \int_{\Omega^e} \mathbf{B}_f^T \mathbf{D}_f \mathbf{B}_f d\Omega^e + \int_{\Omega^e} \mathbf{B}_c^T \mathbf{D}_c \mathbf{B}_c d\Omega^e \tag{20}$$

The mass matrix of the Mindlin plate is then obtained as

$$\mathbf{M}^e = \int_{\Omega^e} \mathbf{\Phi}^T \mathbf{I} \mathbf{\Phi} d\Omega^e \Phi \tag{21}$$

Where $\boldsymbol{\phi}$ is a vector of the shape functions, **I** is the inertia matrix given by

$$\mathbf{I} = \begin{bmatrix} I_0 & 0 & 0 \\ 0 & I_2 & 0 \\ 0 & 0 & I_2 \end{bmatrix} \tag{22}$$

The vector forces **P** is defined as

$$\mathbf{f}^e = \int_{\Omega^e} \mathbf{\Phi} \mathbf{P} d\Omega^e \tag{23}$$

# 3 RPIM meshless method

The RPIM meshless method has been developed based on the point interpolation method (PIM) by including the radial basis function (RPF) in the interpolation formulation and has shown good performance in computational engineering. The accuracy of interpolation for the point of interest depends on the nodes in the support domain. To ensure an efficient and accurate approximation, an appropriate support domain should be chosen. For a point of interest at $x_Q$, the dimension of the support domain $d_s$ is determined by

$$d_S = \alpha d_c \tag{24}$$

Where α is the dimensionless size of the support domain, and $d_c$ is the nodal spacing near the point at $\mathbf{x}_Q$.

Consider a continuous function $u(\mathbf{x})$ defined in a domain Ω, which is represented by a set of field nodes. The u(**x**) at a point of interest **x** is approximated in the form of

$$u(\mathbf{x}) = \sum_{i=1}^{m} p_i(\mathbf{x}) a_i = \begin{Bmatrix} p_1(\mathbf{x}) & p_2(\mathbf{x}) & \dots & p_m(\mathbf{x}) \end{Bmatrix} \begin{Bmatrix} a_1 \\ \vdots \\ a_m \end{Bmatrix} = \mathbf{p}^T \mathbf{a} \tag{25}$$

Where $p_i(\mathbf{x})$ is a given monomial in the polynomial basis function in the space coordinates $\mathbf{x}^T$ = [x, y], $a_i$ is the coefficient for $p_i(\mathbf{x})$ which is yet to be determined, *m* is the number of monomials.

In this study, the quadratic basis functions are used for all numerical computations.

$$\mathbf{p}^T(\mathbf{x}) = \begin{bmatrix} 1 & x & y & x^2 & y^2 & xy \end{bmatrix} \tag{26}$$

# 4 Numerical results

In order to demonstrate the efficiency and the applicability of the present method to static analysis and dynamic analysis problems, the authors present the results obtained from the survey based on an analytical model that combines the theory of S-FSD with the RPIM. Used in the RPIM to integrate the weak form. The boundary conditions of the plate are denoted as follows: simple support (S), clamped (C), and freestyle (F).

Static analysis problems of **FGM** plate

$$\left[\mathbf{K}\right]\left\{\mathbf{d}\right\} = \left\{\mathbf{P}\right\} \tag{27}$$

By using the Hamilton Principle, we may express the equations of motion of Mindlin plates as

$$\mathbf{M\ddot{u}} + \mathbf{Ku} = \mathbf{f} \tag{28}$$

where **M, K, f** are the system mass and stiffness matrices, and the force vector, respectively, and **ü**, **u** are the accelerations and displacements. Assuming a harmonic motion we obtain the natural frequencies and the modes of vibration by solving the generalized eigenproblem

$$\left(\mathbf{K} - \omega^2\mathbf{M}\right)\mathbf{X} = \mathbf{0} \tag{29}$$

where **X** the mode of vibration, representing the vibration pattern corresponding to the eigenvalue $\lambda$. The eigenvalue $\lambda$ is the square of the angular frequency ω, and the frequency $f = \omega/2\pi$ is measured in *Hz* (number of cycles/second). Each frequency value $\omega$ corresponds to a specific type of oscillation. There are many methods of solving a system of equations to find the private vecter and vibration patterns of the system.

## 4.1 Problem 1

The square FGM plate with a sheet thickness of h = *0.01 (m)* is manufactured from material as shown in *Table 1.* It uses the number of nodes *11x11* shown in *Figure 2*, the shear effectiveness factor *K* = 5/6. The RPIM method uses parameters: $\alpha$ = *2.01,* $\Theta$ = *3*. The displacement results of the FGM plate have the above data. The force acting on the FGM plate is a uniformly distributed force with the value P = *1000 (Pa)*. The results of the RPIM method on displacement fields are compared with the COMSOL simulation software presented in *Table 2.* To determine the correctness of the program, the deflection value of the center point of the plate is compared with RPIM and COMSOL software as well as the convergence of the deflection value of the center of the plate through the node sizes *4x4, 10x10, 16x16, 20x20, 26x26,* and *30x30*. They are shown in *Table 3* and *Figure 6, Figure 7 shows the error between RPIM and COMSOL in the* node sizes *10x10.* On the other hand, the first 5 frequencies are also shown in the paper and compared with the results of the COMSOL simulation software, they are shown in *Table 4* and *Figure 8. Table 2* and *Table 3* show that the median displacements of the FGM plate, *Table 4* show the first *5* mode shape of FGM plate, it compared with the results of other methods have an acceptable error (less than *5%*). This error comes from the imposition of the values of the coefficients $\alpha$ and $\Theta$ in the RPIM meshless method. Furthermore, the RPIM meshless method is essentially an interpolation method, so the error problem is not to blame.

| Materials | Young's modulus (Pa) | Poisson's ratio | $\rho$ (kg/m$^3$) |
|---|---|---|---|
| Metal (SUS 304) | *207e9* | *0.3* | *8166* |
| Ceramic ($Al_2O_3$) | *380e9* | *0.3* | *3800* |

**Table 1:** Material properties of FGM plate problem 1

| Boundary conditions | a/h | Method | n | **W** *(e-5m)* | **Θx** *(e-4 rad)* | **Θy** *(e-4 rad)* |
|---|---|---|---|---|---|---|
| CCCC | 100 | RPIM | | 4.7310 | 1.4502 | 1.4502 |
| | | Comsol | 1 | 4.7183 | 1.4660 | 1.4660 |
| | | %(Ml/Cs) | | 0.2684 | 1.0895 | 1.0895 |

**Table 2:** The table shows displacement fields and the error of the two methods

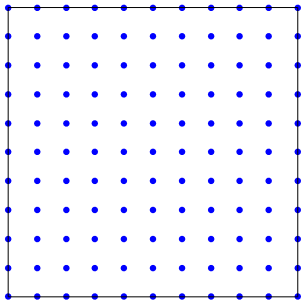

**Figure 2:** Nodal distribution in the square plate with 11x11 regular scattered nodes

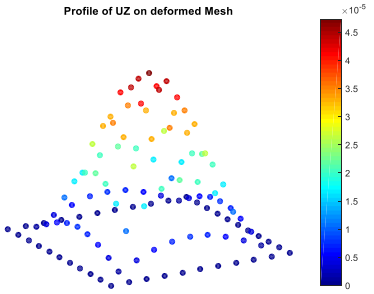


**Figure 3:** The figure shows displacement in the Z direction of the FGM plate size 11x11 nodes

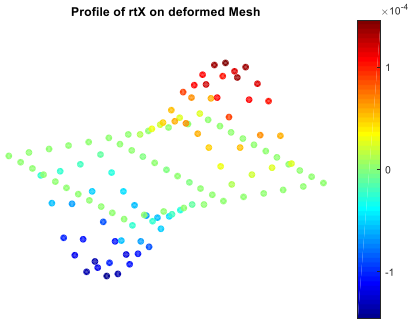


**Figure 4:** The figure shows displacement of the rotation in the X direction of the FGM plate size 11x11 nodes

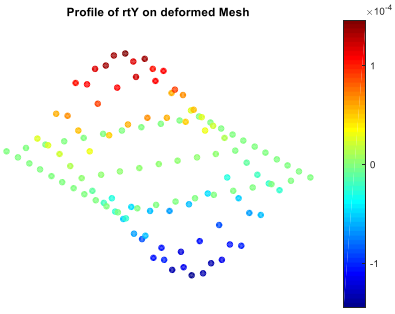


**Figure 5:** The figure shows displacement of the rotation in the Y direction of the FGM plate size 11x11 nodes

Figure 3, Figure 4, and Figure 5 show displacement fields in the Z direction, the rotation in the X direction, and the rotation in the Y direction, respectively. The maximum displacement value in the Z direction at the center of the plate is 4.7310 (e-5m), zero at the four edges. The displacement value of the rotation in the X direction is 1.4502 (e-4rad), the smallest is 1.4502 (e-4rad), equal to 0 at all four edges. The same for the displacement field of the rotation in the Y direction. The total error of the RPIM method is less than 5%.

| Frequency [Hz] | Mode | RPIM | FEM(Comsol) | Error (%) |
|---|---|---|---|---|
| | 1 | 121.16 | 121.25 | 0.0673 |
| | 2 | 245.98 | 247.19 | 0.4915 |
| | 3 | 245.98 | 247.19 | 0.4915 |
| | 4 | 370.08 | 364.12 | 1.6113 |
| | 5 | 438.11 | 443.43 | 1.2131 |

| Boundary conditions | a/h | Method | n | 4x4 | 10x10 | 16x16 | 20x20 | 26x26 | 30x30 |
|---|---|---|---|---|---|---|---|---|---|
| CCCC | 100 | RPIM | 1 | 4.7765 | 4.7310 | 4.7077 | 4.7064 | 4.7077 | 4.7089 |
| | | Comsol | | 4.7629 | 4.7183 | 4.7173 | 4.7151 | 4.7159 | 4.7173 |
| | | %(RPIM/Cs) | | 0.2843 | 0.2684 | 0.2039 | 0.1848 | 0.1741 | 0.1783 |

**Table 3:** The table shows survey of displacement values in the Z direction through the number of nodes

**Table 4:** The table shows the results of calculating the frequencies and the error of the two methods (RPIM and COMSOL)

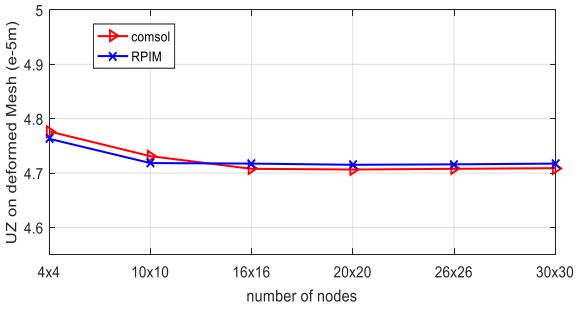


**Figure 6:** The chart shows the change of deflection value of the two methods (RPIM and COMSOL) through the change of node (CCCC)

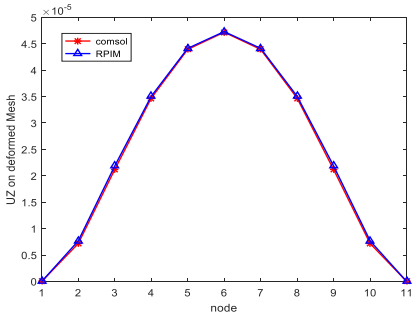


**Figure 7:** Convergence comparisons curves of the central deflection among RPIM and COMSOL for square FGM plate

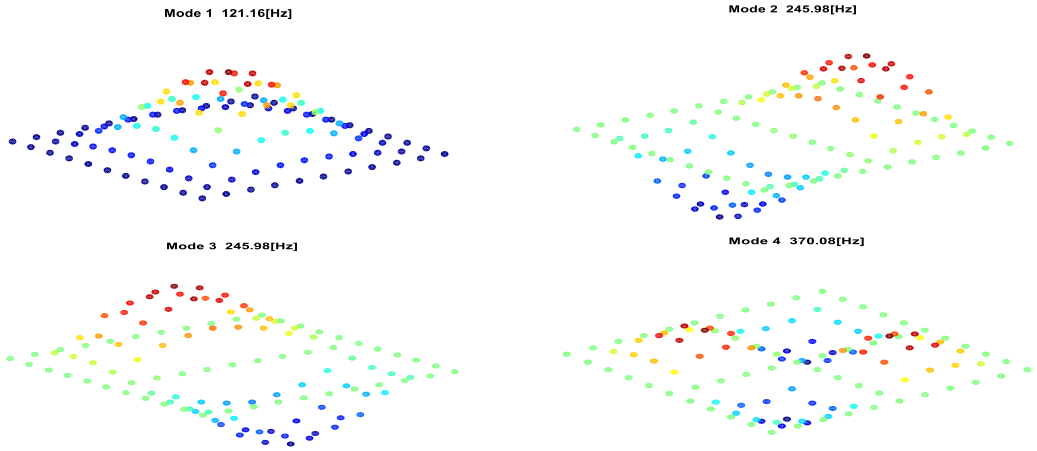

**Figure 8:** The first 4 mode shape of square FGM plate. It is found that the 5-frequency digital terminal corresponds to the 5 frequencies simulated in the commercial simulation software COMSOL

## 4.2 Problem 2

The annulus *FGM* plate with a sheet thickness of h = 0.01 (m) is manufactured from material as shown in Table *5*. The annulus plate has outer diameter $R_1$ = 1 m, inner diameter $R_2$ = 0.2 m and node size of the annulus plate shown in Figure 9. the shear effectiveness factor *K* = 5/6. The RPIM method uses parameters: α = 2.01, Θ = 3. The force acting on the FGM plate is a uniformly distributed force with the value P = 1000 (Pa). The results of the RPIM method on displacement fields are compared with the COMSOL simulation software presented in Table *6.* To determine the correctness of the program in problem 2, the authors change the power-law index to be 1, 5, 10, respectively, to investigate the annulus FGM plate, it shows in Figure 11. On the other hand, the first 5 frequencies are also shown in the paper and compared with the results of the COMSOL simulation software. Table 7 show the first 5 mode shape of FGM plate, it compared with the results of other methods have an acceptable error (less than 5%). This error comes from the imposition of the values of the coefficients α and Θ in the RPIM meshless method. Furthermore, the RPIM meshless method is essentially an interpolation method, so the error problem is not to blame.

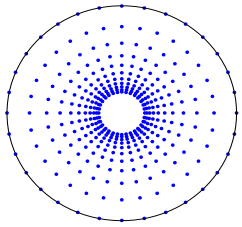

**Figure 9:** Nodal distribution in the annulus FGM plate

| Materials | Young's modulus (Pa) | Poisson's ratio | $\rho$ (kg/m$^3$) |
|---|---|---|---|
| Metal (SUS 304) | *207e9* | *0.3* | *8166* |
| Ceramic ($Al_2O_3$) | *380e9* | *0.3* | *3800* |

**Table 5:** Material properties of FGM plate problem 2

Figure 12, Figure 13, and Figure 14 show displacement fields in the Z direction. The maximum value is *6.1151 (e-4m),* 0 at the outer diameter, (a). The maximum value is *7.2624 (e-4m),* 0 at the outer diameter, (b). The maximum value is *7.7314 (e-4m),* 0 at the outer diameter, (c).The total error of the RPIM method is less than 5%.

| Boundary conditions | a/h | Method | n | **w** *(e-4m)* |
|---|---|---|---|---|
| CCCC | 100 | RPIM | | 6.1151 |
| | | Comsol | 1 | 6.1033 |
| | | %(Ml/Cs) | | 0.1932 |
| CCCC | 100 | RPIM | | 7.2624 |
| | | Comsol | 5 | 7.2454 |
| | | %(Ml/Cs) | | 0.2330 |
| CCCC | 100 | RPIM | | 7.7314 |
| | | Comsol | 10 | 7.7143 |
| | | %(Ml/Cs) | | 0.2210 |

**Table 6:** The table shows displacement fields and the error of the two methods of problem 2

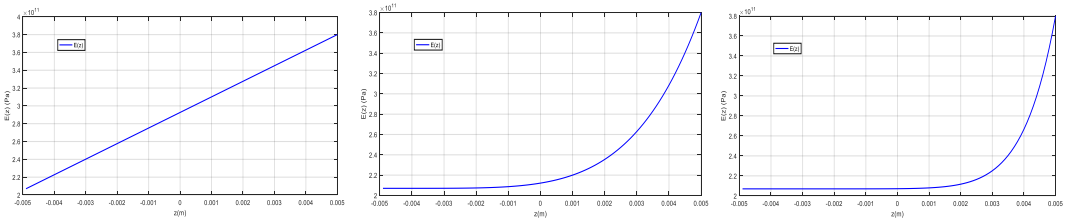

**Figure 10:** The chart shows the change of E(z) with the power-law index, a = 1; b = 5; c = 10.

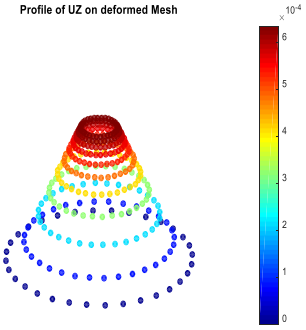


**Figure 11:** The figure shows displacement in the Z direction of the annulus FGM plate (a)

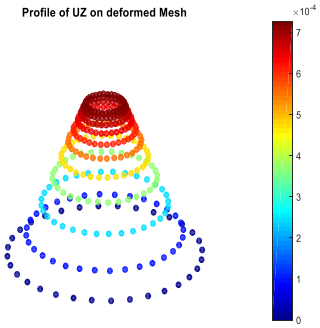


**Figure 12:** The figure shows displacement in the Z direction of the annulus FGM plate (b)

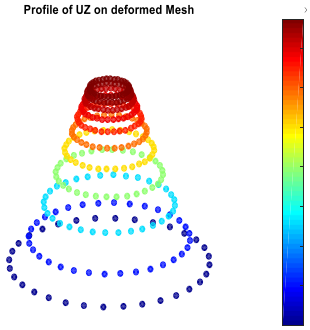


**Figure 13:** The figure shows displacement in the Z direction of the annulus FGM plate (c)

| Frequency [Hz] | Mode | RPIM | FEM (Comsol) | Error(%) |
|---|---|---|---|---|
| | 1 | 34.52 | 34.73 | 0.6083 |
| | 2 | 66.77 | 67.02 | 0.3744 |
| | 3 | 66.77 | 67.02 | 0.3744 |
| | 4 | 108.62 | 111.73 | 2.8631 |
| | 5 | 108.62 | 111.73 | 2.8631 |

**Table 6:** The table shows the results of calculating the frequencies and the error of the two methods RPIM and COMSOL. n =1

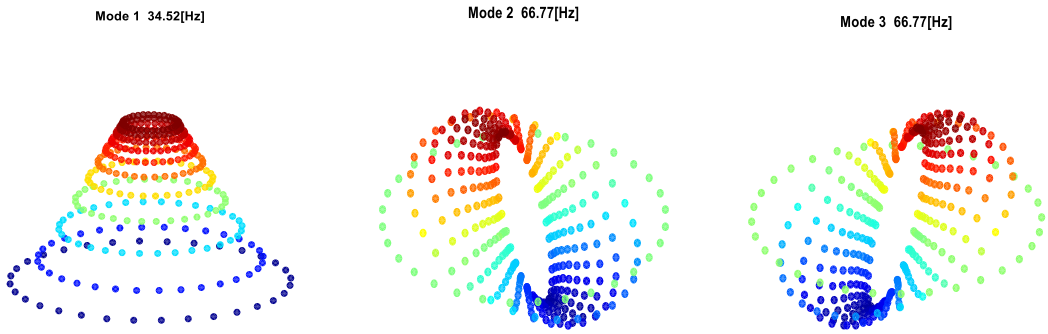

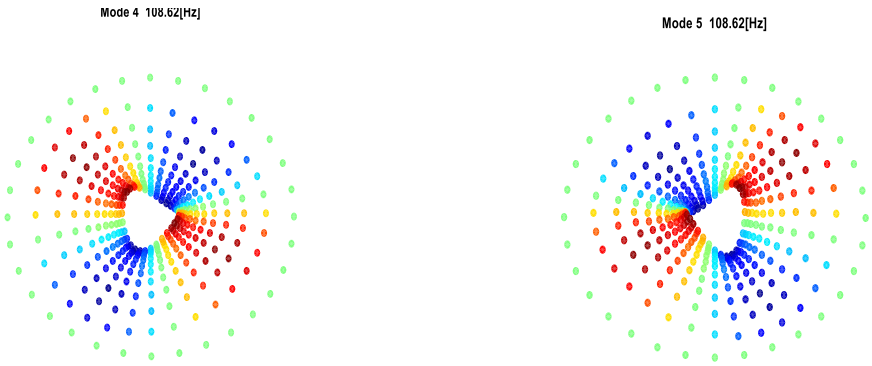


**Table 7:** The first 5 mode shape of annulus FGM plate with n = 1

# 5 Conclusion

The article proposed a displacement calculation model of the FGM plate using an analytical model combining the theory of S-FSD with the RPIM meshless method. Numerical examples of FGM plate displacement are performed and discussed in detail. The factors affecting the displacement of the FGM plate, such as boundary conditions and attenuation index, are also investigated. The results show that using the new proposed model with fewer unknowns but still giving results consistent with the results obtained from the RPIM meshless method, which is used to survey all calculation cases in the paper and always has an error of less than 5%. The method enables us to treat the essential boundary conditions as conveniently as the FEM, effectively and accurately, and its application to other complex problems in FGM structures such as nonlinear analysis, thermal-stress calculation is promising.

# Acknowledgements

This research is funded by Ho Chi Minh City University of Technology (HCMUT), VNU - HCM under grant number SVCQ-2021-KHUD-02. We acknowledge Ho Chi Minh City University of Technology (HCMUT), VNU-HCM for supporting this study.

# References

[1] T. Z. S.N. Atluri, in *A new meshless local Petrov–Galerkin (MLPG) approach in computational mechanics,Computational Mechanics 22*, 1998, p. 117–127.

[2] V. S. C. Z. J. Sladek, Application of meshless local Petrov–Galerkin (MLPG) method to elastodynamic problems in continuously nonhomogeneous solids, Computer Modeling in Engineering and Sciences 4, 2003.

[3] V. S. C. Z. J. Sladek, A meshless local boundary integral equation method for dynamic anti-plane shear crack problem in functionally graded materials, Engineering Analysis with Boundary

Element 29, 2005.

[4] V. S. J. K. P. W. C. Z. J. Sladek, Meshless local Petrov Galerkin (MLPG) method for Reissner-Mindlin plates under dynamic load, Computer Methods in Applied Mechanics and Engineering 196, 2007.

[5] V. S. C. Z. P. S. J. Sladek, Static and dynamic analysis of shallow shells with functionally graded and orthotropic material properties, Mechanics of Advanced Materials and Structures 15, 2008.

[6] Y. T. G. G. R. Liu, An Introduction to Meshfree Methods and Their Programming, 2005.

[7] Y. S. Uflyand, Wave Propagation by Transverse Vibrations of Beams and Plates, PMM: Journal of Applied Mathematics and Mechanics, Vol. 12, 287-300, Russian, 1948.

[8] R. D. Mindlin, Influence of rotatory inertia and shear on flexural motions of isotropic, elastic plates, ASME Journal of Applied Mechanics, Vol. 18 pp. 31–38., 1951.

[9] I. Elishakoff, Handbook on Timoshenko-Ehrenfest Beam and Uflyand-Mindlin Plate Theories, World Scientific, Singapore: ISBN 978-981-3236-51-6, 2020.

[10] I. Andronov, The Analytic Properties and Uniqueness of the Solutions To Problems of Scattering by Compact Obstacles in an Infinite Plate Described by the Uflyand-Mindlin Model, Acoustical Physics, Vol. 53(6), 653-659, 2007.

[11] I. H. F. ,. C. N. Elishakoff, Vibrations of Asymptotically and Variationally Based Uflyand-Mindlin Plate Models, International Journal of Engineering Science, Vol. 116, 58-73, 2017.

[12] A. Loktev, Dynamic Contact of a Spherical Center and Prestressed Orthtropic Uflyand-Mindlin Plate, Acta Mechanica, Vol. 222(1-2), 17-25, 2011.

[13] R. Y. a. S. M.V., Problem of the Impact Interaction of an Elastic Rod With a Uflyand-Mindlin Plate, International Applied Mechanics, Vol. 29(2),, 1993.

[14] R. Wojnar, Stress Equations of Motion for Uflyand-Mindlin Plate, Bulletin de l' Academie Polonaise des Sciences – Serie des Sciences Techniques, Vol. 27(8-9), 1979.

[15] I. Elishakoff, "Generalization of the Bolotin's dynamic edge effect method for vibration analysis of Mindlin plates," Proceedings, the 1994 National Conference on Noise Control Engineering, New York, 1994.

[16] E. Reissner, The effect of transverse shear deformation on the bending of elastic plates, ASME Journal of Applied Mechanics, Vol. 12, pp. A68–77., 1945.

[17] V. S. C. Z. J. Sladek, An advanced numerical method for computing elastodynamic fracture parameters in functionally graded materials, Computational Materials Science 32, 2005.

[18] Y. G. G.R. Liu, "A local point interpolation method for stress analysis of two dimensional solids, Structural Engineering and Mechanics 11," 2001, p. 221–236.

[19] T. Hughes, The Finite Element Method – Linear Static and Dynamic Finite Prentice Hall, Englewood Cliffs, New Jersey, 1987.

[20] Y. G. G.R. Liu, Meshfree Methods, Moving Beyond the Finite Element Method, CRC, U.S.A,

2003.

[21] Y. G. G.R. Liu, "Element free Galerkin method, International," 1994, p. 229–256.

[22] K. Bathe, Finite Element Procedures, Prentice-Hall, Englewood Cliffs, New, 1996.

[23] S. Atluri, The Meshless Local Petrov–Galerkin (MLPG) Method, Tech, Science Press, 2004.